Experimental Comparison of PAM and CAP Modulation for Visible Light Communication Under Illumination Constraints

Robin Le Priol, M. Helard, Sylvain Haese, Sebastien Roy

Experimental Comparison of PAM and CAP Modulation for Visible Light Communication Under Illumination Constraints

Robin Le Priol, *Member, IEEE*, Maryline Hélard, Sylvain Haese, and Sébastien Roy, *Member, IEEE*

***Abstract*—In this paper, we study different modulation techniques for visible light communication (VLC), taking illumination constraints into account. Two modulation schemes are compared, namely pulse amplitude modulation (PAM) and carrierless amplitude and phase (CAP) modulation, through both simulations and experimental measurements. The data link under study is based on low-cost components comprising a white light-emitting diode (LED) and a silicon PIN photodiode. Moreover, the proposed VLC system complies with illumination standards and limits the brightness level to that of a typical office room. The impact of the roll-off factor parameter, which is directly related to the total occupied bandwidth, and the maximum achievable throughput for PAM and CAP are studied. Moreover, adaptive postdistortion based on a Volterra series expansion is implemented to mitigate the effects of LED nonlinearity in practice. We also demonstrate that 8-PAM can outperform 64-CAP and discrete multitone (DMT) when the LED nonlinearity is adequately compensated.**

***Index Terms*—Visible light communication (VLC), light-emitting diode (LED) lighting, pulse amplitude modulation (PAM), carrierless amplitude and phase (CAP) modulation, discrete multitone (DMT), indoor illumination.**

I. Introduction

VISIBLE light communication (VLC) is an emerging optical communication technology based on the use of light-emitting diodes (LED) to simultaneously deliver illumination and communication functions. VLC has drawn a lot of attention in recent years and is expected to become a viable alternative to radio frequency systems, as it provides many advantages such as immunity to electromagnetic interference, intrinsic robustness against eavesdropping, and low-cost transceivers based on commercially available components [1]–[3]. The optical bands of the electromagnetic spectrum also offer approximately 375 THz of license-free bandwidth, thus providing ample room to relieve pressure on the radio spectrum. Moreover, currently deployed lighting fixtures can be leveraged to implement VLC since white LEDs are nowadays widely used for lighting applications [4]. Common white LEDs (unlike the more expensive red-green-blue (RGB) LEDs) consist of a blue LED chip coated with a phosphor layer, producing white light. Unfortunately, their modulation bandwidth does not exceed a few MHz due to the relaxation time of the phosphor layer, thus severly limiting throughput [5]. To overcome this, spectrally-efficient signaling schemes are commonly considered in VLC, such as pulse amplitude modulation (PAM), carrierless amplitude and phase modulation (CAP), and discrete multitone (DMT).

In fact, two main approaches are generally considered regarding the use of bandwidth. In the first one, the signal is narrowband and modulated using single-band modulation schemes such as CAP or PAM. In this case, the achieved transmission rate is low and the channel is assumed to be non-frequency-selective, thus no equalization is required. In the second approach, the information signal is wideband to improve the bit rate and multi-band modulation schemes such as multi-band CAP or DMT-based techniques are employed in combination with adaptive bit-loading while avoiding complex equalization.

Comparisons of PAM, CAP and DMT have been carried out in the literature for VLC in terms of available bitrates and robustness against LED nonlinear distortions. In [6], the authors compared PAM, CAP and DMT on an experimental setup employing a white LED. Under different signal attenuations, they highlighted the robustness of two-level PAM (2-PAM) against LED nonlinearities, which performed advantageously with respect to CAP and DMT. The authors of [7] compared high-order PAM (8-PAM) and CAP (64-CAP) with DMT employing frequency domain equalization. They reported better performance for DMT compared to high-order PAM and CAP. Moreover, CAP outperformed PAM for high data rates. In [8], the authors performed an optimization of the roll-off factor and demonstrated that 4-PAM can outperform 4-CAP and DMT.

It is noteworthy, however, that none of these studies took into account the constraints associated with the illumination function. VLC systems employ intensity-modulation and direct-detection (IM/DD), where the transmitted waveform is encoded in the instantaneous radiated optical power. In this context, the desired illumination brightness level limits the total optical power at the receiver, thus impacting communication link quality. Moreover, the authors of [7] and [8] did not consider a nonlinear LED dynamic range and did not provide experimental results, yet it is known that LED nonlinear distortions can

Manuscript received November 22, 2021; revised January 14, 2022; accepted January 28, 2022. Date of publication February 4, 2022; date of current version February 25, 2022. *(Corresponding author: Robin Le Priol.)*

Robin Le Priol, Maryline Hélard, and Sylvain Haese are with the Université de Rennes, INSA Rennes, CNRS, IETR - UMR 6164, F-35000 Rennes, France (e-mail: robin.le-priol@insa-rennes.fr; maryline.helard@insa-rennes.fr; sylvain.haese@insa-rennes.fr).

Sébastien Roy is with the Department of Electrical and Computer Engineering, University of Sherbrooke, Sherbrooke, QC J1K 2R1, Canada (e-mail: sebastien.roy13@usherbrooke.ca).

Digital Object Identifier 10.1109/JPHOT.2022.3148467

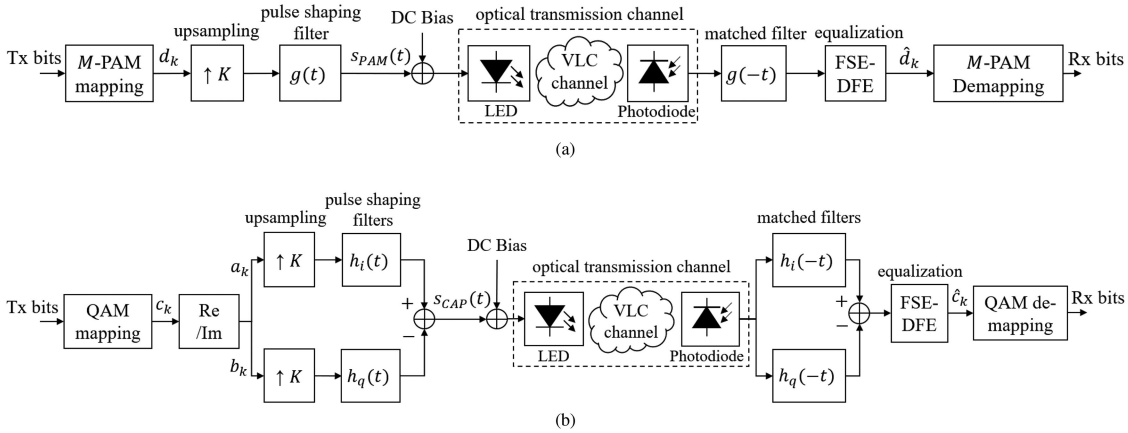

Fig. 1. Schematic block diagrams of (a) PAM and (b) CAP transceivers for VLC.

severely degrade overall system performance [9]. It is reasonable to assume that modulations with higher peak-to-average power ratio (PAPR) will suffer more degradation due to nonlinearity. In previous work by our team [10], DMT was optimized under lighting constraints with the same experimental VLC setup and a 100 Mbps transmission was achieved at a targeted bit error rate of 10^{-3}. Therefore, this study focuses on optimization and comparison of PAM and CAP.

In this paper, we study the impact of different parameters of single-band CAP and PAM when extending as much as possible the signal bandwidth while employing equalization and/or post-distortion techniques to jointly mitigate the frequency selectivity and the nonlinear effects of the LED. Given that the transmitted signal spectrum is not bounded by neighboring channels, the modulation bandwidth in VLC is a parameter that can be freely optimized without being constrained by overlapping spectra, as opposed to radio frequency systems where the electromagnetic spectrum is strictly regulated. In addition, a constant brightness level that is compliant with illumination standards is maintained at the receiver level. Moreover, given that a low signal PAPR is usually preferred to optimize the occupation of the LED dynamic range and thus maximize the transmit power, PAM and CAP were chosen over multi-band CAP and DMT-based techniques which are known to exhibit higher PAPR.

For both CAP and PAM schemes, the impact of the roll-off factor and the maximum achievable bit rate is investigated in simulation while assuming a perfectly linear LED dynamic range. In addition, an experimental transmission is performed to study the performance of high-order 8-PAM and 64-CAP with and without compensation of the LED nonlinearity.

In our study, the average optical power is kept constant for all modulated signals to set the desired level of illumination. However, the electrical signal powers are different, since the modulated signals occupy the entire dynamic range of the LED as opposed to [6]. In addition and as opposed to [8], higher modulation orders will be studied, namely 8-PAM and 64-CAP and the LED nonlinearity will be integrated into the study by experiment.

The remainder of the paper is organized as follows: Section II presents an analytical description of PAM and CAP modulation. Section III presents a simplified model of the experimental VLC link, the electro-optical LED transfer characteristic and the illumination requirements. In Section IV, the impact of the roll-off factor parameter is investigated, along with the maximum bit rate for different modulation orders. In Section V, an experimental transmission is performed to highlight the effects of LED nonlinearity. Finally, Section VI concludes the paper.

II. Modulation Schemes

The two modulation schemes compared in this paper are PAM and CAP. An analytical description of PAM is given in Section II-A, while CAP is presented in Section II-B.

A. PAM Modulation

PAM is a modulation scheme where the information is encoded in the amplitude of the transmitted pulse. Here, a square-root raised-cosine (SRRC) pulse shaping filter is employed to optimize spectral occupancy. Fig. 1(a) shows a schematic of a PAM transceiver. The incoming bits are firstly modulated by a PAM modulator where the signal levels are defined as $\pm 1, \pm 3, \ldots, \pm M-1$, and where M is the modulation order. Then, the modulated symbol stream d_k is upsampled by a factor K and convolved with a SRRC filter $g(t)$, yielding the transmitted PAM signal

$$s_{PAM}(t) = \sum_{k=-\infty}^{+\infty} d_k g(t - kT), \tag{1}$$

where T is the symbol period. The PAM modulation bandwidth B_{PAM} is therefore limited by the maximum frequency of the pulse shaping filter $g(t)$, such that

$$B_{PAM} = \frac{(1+\alpha)}{2\,T} = \frac{(1+\alpha)D_b}{2m_{PAM}}, \tag{2}$$

where α is the roll-off factor parameter denoting the excess bandwidth, D_b is the bit rate and m_{PAM} is the number of bits encoded in one PAM symbol. The PAM modulated spectrum for various values of α and the LED frequency response are shown in Fig. 2(a). Then, a DC bias is added for illumination purposes and to ensure full swing of the modulated signal in the dynamic range of the LED. At the receiver side, the received signal is passed through the matched filter $g(-t)$ prior to equalization. The equalizer employed in this study is a fractionally-spaced

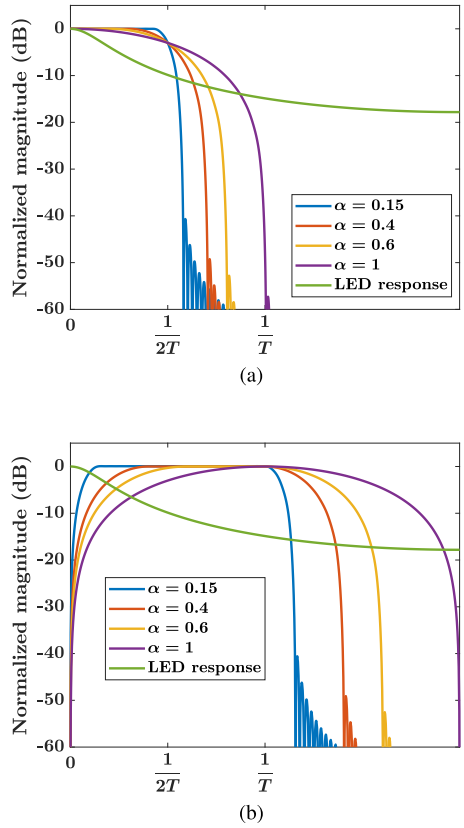

Fig. 2. PAM (a) and CAP (b) modulated spectra for various roll-off factors and LED normalized frequency response.

decision-feedback equalizer (FSE-DFE) operating at the rate $4/T$. The upsampling factor K is set to 4 in this study, thus providing an appropriate tradeoff between performance and complexity. It is noteworthy that the feedforward part of the equalizer operates at the same rate as the upsampled signal, therefore the received signal is not downsampled prior to equalization. The downsampling operation is integrated into the equalization block as detailed in [11]. The equalizer output, however, delivers equalized symbols $\hat{d}_k$ at symbol rate $1/T$. Finally, the equalized PAM symbols are de-mapped in order to recover the transmitted bits stream.

B. CAP Modulation

CAP modulation was historically developed for communication over copper wires [12] and has drawn a lot of interest recently for its potential as a suitable modulation for VLC. In CAP, a pair of finite impulse response filters is used to transmit an in-phase and a quadrature component in an orthogonal fashion [13]. An interesting property of CAP is that the baseband signal spectrum is shifted upwards (as with a carrier) but the amount of shift f_c is low and is such that the resulting spectrum remains in the baseband domain, i.e. the lower side band extends near or at $f = 0$.

It is worth mentioning that CAP can be extended to a multi-band modulation format, namely multi-band CAP, where the signal bandwidth is divided into sub-bands. By virtue of lowering the bandwidth requirement for each sub-band, the attenuation over the signal frequencies due to the low-pass channel is reduced. Furthermore, adaptive bit-loading can be applied to optimize the constellation size on each sub-band depending on the channel attenuation and improve the spectral efficiency. Nevertheless, it was shown in [13] that a drawback of multi-band CAP is the PAPR, which grows with the number of sub-bands. Considering the limited LED dynamic range, a power penalty can be induced at the transmitter.

The CAP signaling scheme is illustrated in Fig. 1(b). First, the incoming bits are modulated into quadrature amplitude modulation (QAM) symbols c_k. Then, the real and imaginary parts a_k and b_k are separated, upsampled by a factor K and convolved with the filters $h_i(t)$ and $h_q(t)$, respectively. The filter outputs are then subtracted, yielding the CAP signal $s_{CAP}(t)$ defined as

$$s_{CAP}(t) = \sum_{k=-\infty}^{+\infty} a_k h_i(t - kT) - b_k h_q(t - kT), \quad (3)$$

The in-phase filter $h_i(t)$ and quadrature filter $h_q(t)$ are obtained by multiplying a cosine of frequency f_c with the same SRRC filter $g(t)$ as in PAM, such that

$$h_i(t) = g(t)cos(2\pi f_c t), \quad (4)$$

and

$$h_q(t) = g(t)sin(2\pi f_c t). \quad (5)$$

The center frequency of the CAP signal spectrum is denoted f_c. In order to avoid any aliasing, f_c must be equal or greater than the maximum frequency of $g(t)$. Furthermore, it is desirable to maximize occupancy of the LED 3-dB modulation bandwidth, leading us to define f_c as being equal to the said maximum frequency, i.e.

$$f_c = \frac{(1+\alpha)}{2\,T}. \quad (6)$$

The total occupied bandwidth B_{CAP} is therefore equal to

$$B_{CAP} = \frac{(1+\alpha)}{T} = \frac{(1+\alpha)D_b}{m_{CAP}}, \quad (7)$$

m_{CAP} being the number of bits per symbol in CAP. The shape of the CAP modulated spectrum for various values of α and the LED frequency response is shown in Fig. 2(b). At the receiver side, the signal is convolved with the matched filters $h_i(-t)$ and $h_q(-t)$. The in-phase part and quadrature part are then recombined to obtain complex QAM symbols prior to equalization with FSE-DFE and QAM de-mapping.

C. Spectral Efficiency of PAM and CAP

The spectral efficiency is generally defined as the ratio between the bit rate D_b and the total occupied bandwidth B such that

$$\eta = \frac{D_b}{B}. \quad (8)$$

Thus, the spectral efficiencies of PAM and CAP can be derived using (8), Eq. (2) and Eq. (7) as follows:

$$\eta = \frac{m_{CAP}}{(1+\alpha)} = \frac{2m_{PAM}}{(1+\alpha)}. \quad (9)$$

When comparing PAM and CAP modulations at same spectral efficiency, we can note that a higher modulation order will be required for CAP compared to PAM modulation. In fact, the number of bits per symbol in CAP needs to be twice that of PAM such that $m_{CAP} = 2m_{PAM}$.

III. VLC Link Model and Assumptions

A. LED Frequency Response Model

The LED impulse response is the main limitation with respect to the modulation bandwidth in the VLC channel. The white LED produces white light by combining blue photons that are emitted directly by the blue chip and the photons re-emitted by the phosphor layer that covers the LED chip.

Therefore, the overall LED response can be modeled as the sum of two channels: the first channel $h_b(t)$ corresponds to the blue light response while the second channel $h_p(t)$ corresponds to the phosphor layer response. The overall LED impulse response can be written as [8], [14]

$$h_{LED}(t) = G_b h_b(t) + G_p \left(h_p(t) * h_b(t)\right), \tag{10}$$

where $*$ denotes the convolution operator and G_b and G_p are the power gains associated with the blue light response and the phosophor layer response respectively. Under the assumption that most of the received optical power stems from the yellow photons [15], we have $G_p \gg G_b$ and a simplified model of the LED response can be derived from (10), such that

$$h_{LED}(t) = G_p \left(h_p(t) * h_b(t)\right). \tag{11}$$

The responses $h_b(t)$ and $h_p(t)$ can be modeled as simple first order low-pass filters [16], i.e.

$$\begin{aligned} h_b(t) &= u(t)e^{-2\pi f_b t}, \\ h_p(t) &= u(t)e^{-2\pi f_p t}, \end{aligned} \tag{12}$$

where f_b and f_p are the 3-dB cut-off frequencies of the blue light response and the phosphor layer response, respectively, and $u(t)$ is the unit step function.

The LED device selected for this study is a low-cost white LED (Lumiled LUXEON 3020) with a color temperature of 3000 K typically used for lighting applications with a 3-dB modulation bandwidth measured at 1.47 MHz. The cut-off frequencies f_b and f_p are estimated at 12 MHz and 1.47 MHz respectively.

The LED frequency response is obtained by taking the Fourier transform of (11), yielding

$$H_{LED}(f) = G_p \cdot \frac{1}{1 + j\left(\frac{f}{f_b}\right)} \cdot \frac{1}{1 + j\left(\frac{f}{f_p}\right)}. \tag{13}$$

It is noteworthy that G_p is set to 1 in order to normalize the frequency response ($H(0) = 1$). The frequency response of the LED was measured with a network analyzer (HP-4195 A) and compared with that of the proposed model in (13) in Fig. 3. It can be observed that the magnitude response of the proposed model fits closely with the measured one. Therefore, the former

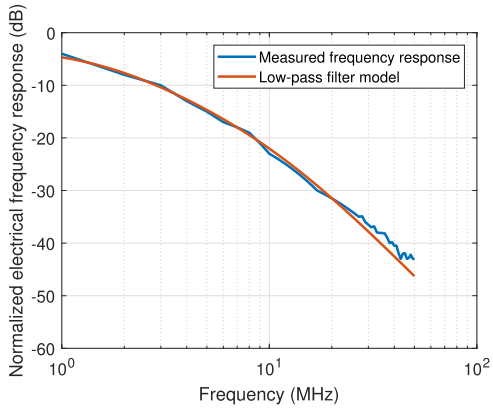

Fig. 3. Measured LED magnitude response and proposed analytical model.

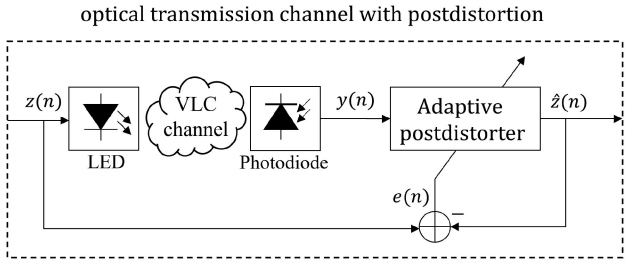

Fig. 4. Principle of adaptive postdistortion for LED nonlinearity mitigation in VLC.

is assumed to be a reasonable approximation of the low-pass behavior of the chosen LED device in this study.

The maximum system bandwidth under study is limited to 50 MHz in this work since the electronic components selected for the LED driver and the receiver, namely the amplifiers, have a limited bandwidth. In addition, the low-pass filter model of the VLC link would be inaccurate beyond this upper bound. Therefore, the received signal $y(t)$ can be expressed as

$$y(t) = \gamma s(t) * h_{LED}(t) + n(t), \tag{14}$$

where $s(t)$ is the PAM or CAP modulated signal, γ is a transfer DC gain between the input and output of the VLC experimental testbed (empirically determined to be 2.9) and $n(t)$ is the additive noise, which is Gaussian-distributed with zero mean and is considered white over the bandwidth of interest (i.e., 50 MHz). The unilateral power spectral density (PSD) of the noise N_0 measured at the output of the VLC receiver is equal to -116 dBm/Hz.

B. LED Nonlinearity and Adaptive Volterra-Based Postdistorter

The LED electro-optical transfer characteristic relating the forward current and the output optical power is a nonlinear function as can be seen in Fig. 5 for the case of the white LED considered in this study. The forward current dynamic range spans from 0 to 240 mA and the bias current is 120 mA, which are typical values recommended by the LED manufacturer. When full swing of the modulated input current is enforced, the variations of radiated optical power with respect to the driving

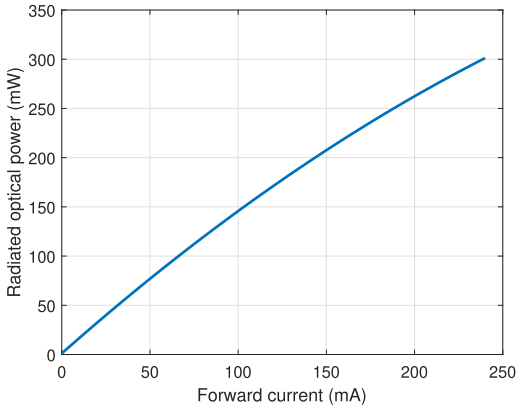

Fig. 5. Lumiled LUXEON 3020 electro-optical static transfer function.

signal cause signal distortions which degrade the overall performance of the system. In addition, the nonlinear LED transfer characteristic includes a memory effect which grows with the signal bandwidth [17], [18]. As a matter of fact, the nonlinear behavior of the LED cannot be neglected at high transmission rates. Furthermore, The LED characteristics may vary over time due to thermal effects and aging of the component.

A linear transfer characteristic is assumed in our simulation model. However, in the experiment, adaptive postdistortion must be applied to compensate the nonlinear impairements and thus linearize the VLC system. Several linearization approaches have been proposed in previous works for that purpose, including the Volterra series model [19], [20], the memory polynomial model [21], or more recently, machine learning algorithms [22]–[24]. In this study, the second-order Volterra series model is implemented, as it provides good performance at high data rate [25].

A diagram of the adaptive postdistortion method is presented in Fig. 4. The output of the Volterra-based postdistorter $\hat{z}(n)$ can be be expressed as [26]

$$\hat{z}(n) = \sum_{k=1}^{K} \sum_{m_1=0}^{M-1} \cdots \sum_{m_k=0}^{M-1} h_k(m_1, \ldots, m_k) \prod_{l=1}^{k} y(n - m_l), \tag{15}$$

where $y(n)$ is the discrete-time received signal, K is the nonlinear order of the Volterra series expansion, M is the memory length and $h_k(m_1, \ldots, m_k)$ is the Volterra kernel of k-th order at time delay m_k. Third-order and second-order Volterra series have been investigated by the authors of [27], and it was concluded that second-order kernels of the Volterra-series expansion lead to a fairly precise approximation of white LED nonlinear distortions. Therefore, in this study, only the terms up to the 2nd kernel order and (15) can be further simplified such that

$$\hat{z}(n) = \sum_{m_1=0}^{M-1} h_1(m_1) y(n - m_1) + \sum_{m_1=0}^{M-1} \sum_{m_2=0}^{M-1} h_2(m_1, m_2) y(n - m_1) y(n - m_2), \tag{16}$$

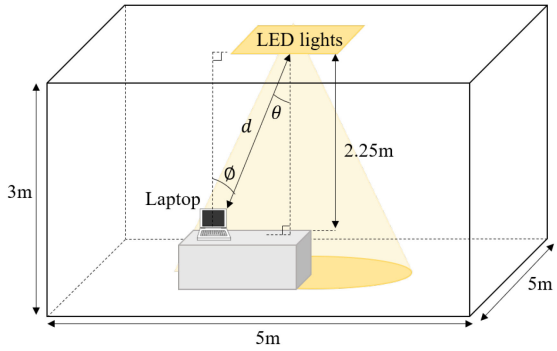

Fig. 6. VLC transmission in a typical office room.

The optimum coefficients $h_k(m_1, \ldots, m_k)$ are adaptively determined by using the recursive least squares (RLS) algorithm [25], which minimizes the least squares cost function defined as

$$\underset{h_k(m_1,\ldots,m_k)}{\operatorname{argmin}} \sum_{n=0}^{M-1} \mid z(n) - \hat{z}(n) \mid^2, \tag{17}$$

where $z(n)$ is the transmit sequence of undistorted symbols.

C. Illumination Constraint

When assessing the illumination distribution in space of a LED-based luminaire, an important metric is the horizontal illuminance E_h which is defined as the luminous flux per unit area [lm/m^2] and is measured in lux (lx). Assuming that the LED has a Lambertian radiation pattern, the horizontal illuminance is given by the following expression [28]:

$$E_h = (m+1) \frac{cos^m(\theta) cos(\phi)}{2\pi d^2} \Phi, \tag{18}$$

where θ is the angle of emission relative to the axis normal to the transmitter surface, ϕ is the angle of incidence of the light relative to the axis normal to the receiver surface, and d is the distance between transmitter and receiver as depicted in Fig. 6 which represents a typical office room of size $5 \times 5 \times 3$ m^3. The Lambertian emission order m is defined by $m = \dfrac{-ln2}{ln(cos(\theta_{\frac{1}{2}}))}$, $\theta_{\frac{1}{2}}$ being the semi-angle at half luminance of the LED (equal to 55°in our study).

According to European norm EN 12464-1 for lighting of indoor work places, a horizontal luminance of 500 lx must be ensured at the user level to read and write in a typical office room [29]. In such a scenario, a luminaire made of multiple LEDs would be employed to achieve the desired illumination level, since a single LED provides a limited luminous flux. The chosen LED for this study outputs a luminous flux of 53 lm when the bias current is set to 120 mA.

Moreover, a distance of 2.25 m typically separates a desk from the ceiling. When the desk is placed right below the roof-mounted luminaire in the center of the room (i.e., $\theta = \phi = 0$), the luminous flux required to achieve 500 lx at the user level is 7078 lm according to (18). It is assumed that all LEDs in the luminaire are located at the same point for the sake of simplicity.

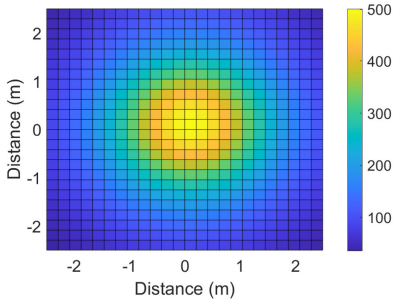

Fig. 7. Horizontal luminance on the receiver plane at a distance of 2.25 m from the ceiling.

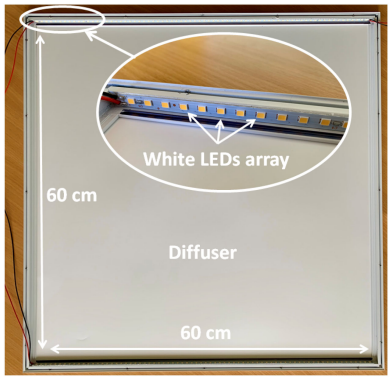

Fig. 8. Typical LED light fixture used for indoor illumination (Sylvania START Panel Flat UGR19 600x600 Neutral White). This typical panel consists of 144 total mid-power LEDs and outputs a luminous flux of 3500 lm.

Therefore, 134 LEDs of the selected type would be required to achieve the desired illumination level. The horizontal luminance on the receiver plane at a distance of 2.25 m from the ceiling is shown in Fig. 7.

As depicted in Fig. 8, light fixtures employed for indoor illumination typically comprise multiple mid-power LEDs (such as the one we selected in this study) instead of a single high-power LED in order to facilitate heat dissipation and improve electro-optical conversion efficiency. If a diffuser is used in the luminaire as in Fig. 8, the distribution of luminance will be more homogeneous and the number of LEDs must be increased to obtain a luminance of 500 lx at the receiver location. However, in order to reduce the size and complexity of the experimental setup, we use a single LED while still ensuring the desired level of illumination at the receiver side. Thus, using (18), the illumination requirement of 500 lx using one LED is fulfilled when the link length is set to 20 cm. Note that the bandwidth limitation and nonlinear behavior of the VLC system are taken into account, and the results of this study can naturally be extended to an implementation scenario in a typical office room using a luminaire with a larger number of similar LEDs.

IV. Numerical Analysis

A. Impact of Roll-Off Factor

The roll-off factor α of the SRRC pulse shaping filter (for PAM) and the in-phase and quadrature filters (for CAP) can be jointly optimized with the modulation bandwidth in order to maximize the system throughput. The roll-off factor impacts the modulated signal on two important fronts, namely 1) the spectral energy distribution and 2) the PAPR.

1) Spectral Energy Distribution: In PAM, most of the energy of the modulated spectrum is concentrated in the low frequencies. Therefore, when increasing the modulation bandwidth (hence, the data rate) beyond the 3-dB bandwidth of the LED, about the same power loss is experienced regardless of roll-off factor. On the other hand, the power in the CAP spectrum is concentrated around f_c and there is no energy at $f = 0$. Therefore, the CAP signal is more subject to power losses due to the LED low-pass behavior than PAM modulation. Moreover, in CAP, larger values of α lead to higher attenuation.

2) PAPR: A low PAPR is preferred in order to enable full swing of the modulated signal in the fixed dynamic range of the LED, and thus to maximize the transmitted electrical power. The PAPR is defined as the ratio between the instantaneous electrical power $s(t)^2$ and the average electrical power $\mathbb{E}[s(t)^2]$ of the transmitted signal, i.e.

$$PAPR = 10\log_{10}\left(\frac{s(t)^2}{\mathbb{E}[s(t)^2]}\right). \tag{19}$$

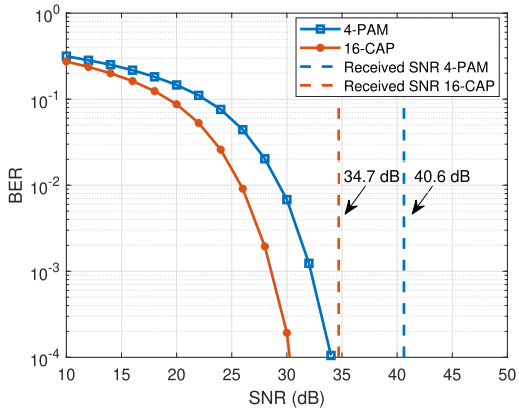

Fig. 9. BER performance of 4-PAM and 16-CAP at 172.5 Mbps with $\alpha = 0.15$ and estimated received SNR for each modulation scheme.

B. Maximum Throughput Investigation

In order to evaluate the maximum bit rate of PAM and CAP in simulation, we define the power margin as the difference between the estimated signal-to-noise ratio (SNR) at the receiver after transmission through the VLC system and the SNR required to achieve a BER of 10^{-3} at a given bit rate. To this extent, a power margin superior to 0 dB implies a transmission at a BER $\leq 10^{-3}$ for an illumination of 500 lx.

In order to illustrate the notion of power margin, the BER performance of 4-PAM and 16-CAP as a function of SNR and at a throughput of 172.5 Mbps is presented in Fig. 9. The received SNR after transmission for 4-PAM and 16-CAP is represented by vertical dashed lines and is equal to 34.7 dB and 40.6 dB, respectively. In addition, the SNR required to achieve a BER of 10^{-3} is $\sim$ 32.2 dB for 4-PAM and $\sim$ 28.6 dB for 16-CAP. Consequently the power margin is equal to 8.4 dB and 6.1 dB for 4-PAM and 16-CAP, respectively.

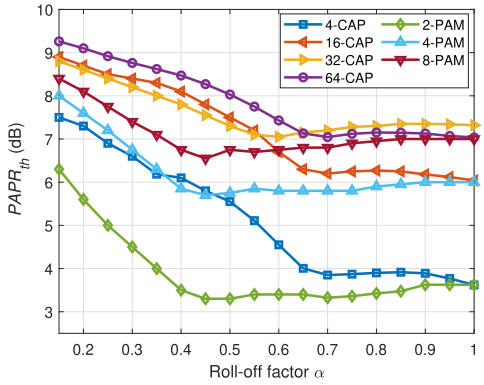

Fig. 10. PAPR threshold of PAM and CAP signals for a probability P_r that $P_r(PAPR > PAPR_{th}) = 10^{-4}$ for various roll-off factors.

The results for different power margins according to different values of α are shown in Fig. 11. It should be noted that the dashed red line on the graphs correspond to the 50 MHz bandwidth bound of the VLC system as explained in Section III-A. For example, as illustrated in Fig. 11(a), for a 2-PAM signal and assuming a 50 MHz total occupied bandwidth, a 86.25 Mbps transmission at a BER lower than 10^{-3} can be achieved with a 0.15 roll-off factor and a very comfortable 18.4 dB margin. On the other hand, a transmission rate of only 72.5 Mbps is achievable given a 0.4 factor roll-off, albeit with a higher margin equal to 24.3 dB. It is of interest that for higher modulation bandwidths (obtainable with better electronic components), the red line would move upwards, indicating higher possible throughputs.

The following observations can be drawn from Fig. 11

- *For PAM:* it can be noticed in Fig. 11(a), (b) and (c) that, for a given power margin, the maximum bit rate is achieved for $\sim \alpha = 0.4$, i.e., when the PAPR is the lowest, as can be seen in Fig. 10. Under this condition, the input LED driving signal can span the full LED dynamic range and thus the transmitted electrical power can be maximized. Consequently, the power margin is increased, and a higher achievable bit rate can be achieved. It can also be seen that the PAPR slightly increases when α approaches 1 (on the order of 0.5 dB) which accounts for the slightly decreasing bit rate in Fig. 11(a), (b) and (c).
- *For CAP:* as opposed to PAM; the power loss experienced by the signal after filtering by the LED impulse response increases with the value of α. This can be directly seen in Fig. 2(b) which shows the shape of the CAP modulated spectrum for various values of α and the LED frequency response. As the roll-off increases, the signal spectrum is shifted around a frequency $f_c = (1+\alpha)/2\,T$ and is subject to a stronger attenuation after filtering by the LED response. On the other hand, the decreasing PAPR leads to more power at the receiver. In fact, the PAPR of CAP signals decreases when the roll-off factor increases to reach its minimum value for $\alpha = 0.6$ for 4-CAP, 16-CAP and 64-CAP and around 0.55 for 32-CAP as observed in Fig. 10. The power gain inherent to the decreasing PAPR does not compensate the power loss due to the attenuation of the LED which accounts for the monotonically decreasing curves in Fig. 11(d), (e) and (f).

In addition, the maximum bit rate for PAM and CAP in a maximum bandwidth of 50 MHz can be achieved with a small value of α, typically 0.15, which yields both a positive power margin and a minimal bandwidth requirement. Moreover, PAM provides a power margin gain on the order of 2-3 dB and 1-2 dB for 2-PAM and 4-PAM, with respect to 4-CAP and 16-CAP, respectively.

Finally, 8-PAM and 64-CAP are compared and revealed to approximately provide similar total throughput with a slight advantage of $\sim$ 1 dB in power margin for 8-PAM. In addition, simulation results (not shown in figure) show that 64-CAP exhibits slightly higher performance than 32-CAP: in fact, for a bit rate of 210 Mbps, 64-CAP exhibits a power margin of 3.85 dB compared to 3.45 dB for 32-CAP.

V. Experimental Results

In this section, an experimental transmission is performed to verify the simulation results for high modulation orders (8-PAM and 64-CAP). Adaptive postdistortion based on the Volterra series expansion is employed to mitigate the LED nonlinearity distortion. Performance without postdistorsion is also assessed to evaluate the degree of sensitivty to nonlinear impairements. In addition, a transmission with bit-loading DMT is performed for comparison with PAM and CAP. As DMT is not a main focus of this paper, this is done to provide a comparative benchmark representing this popular modulation scheme.

A. Experimental Setup

Fig. 12(a) and (b) show a diagram and a picture of the experimental setup, respectively. The VLC transmission proceeds as follows. Firstly, the PAM and CAP signals are generated offline with MATLAB and stored into an arbitrary waveform generator memory (Tektronix, AWG7052TM, 10 bits resolution). The latter performs a digital-to-analog conversion, and the output modulated signal is combined with a DC bias current by means of a custom board to provide the right level of illumination and to ensure that the driving signal occupies the entire LED dynamic range.

At the receiver side, a 16-mm diamter lens concentrates the light onto a low-cost silicon PIN photodiode (OSRAM SFH-2400) with a 1 mm^2 active surface. The photodiode produces a photocurrent proportional to the received optical power, which is then converted into a voltage signal using a transimpedance amplifier circuit. The received signal is finally sampled by a real-time oscilloscope (LeCroy 64 MXs-A), digitized and saved for subsequent offline processing. The latter includes resampling, synchronization, postdistortion, matched filtering, FSE-DFE equalization, symbol de-mapping and BER calculation. The system parameters used in the experiment are summarized in Table I.

B. Impact of LED Nonlinearity

In order to highlight the effect of nonlinear characteristic of the LED on high-order PAM and CAP, transmissions with 64-CAP and 8-PAM were performed and the constellation and eye diagrams with and without postdistortion are shown in

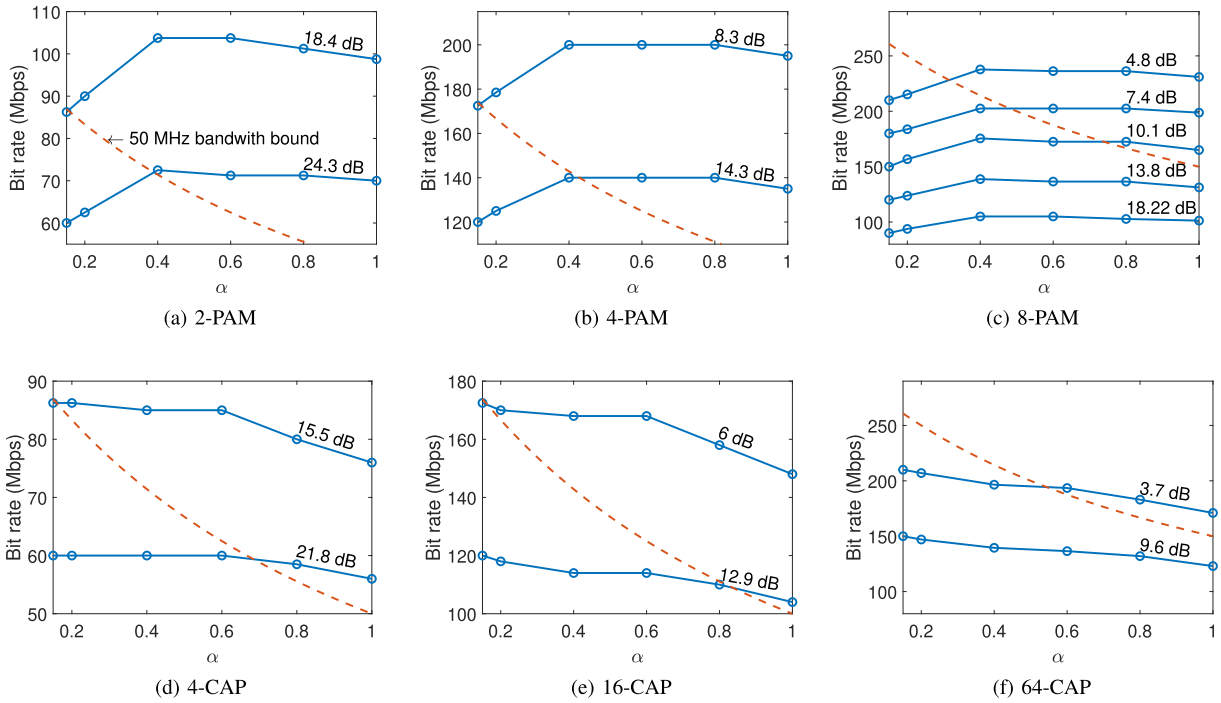

(a) 2-PAM (b) 4-PAM (c) 8-PAM

(d) 4-CAP (e) 16-CAP (f) 64-CAP

Fig. 11. Achievable bit rate for (a) 2-PAM, (b) 4-PAM, (c) 8-PAM, (d) 4-CAP, (e) 16-CAP, and (f) 64-CAP for a given power margin according to various values of roll-off factor. The dashed red curve on the plots corresponds the bandwidth boundary of 50 MHz.

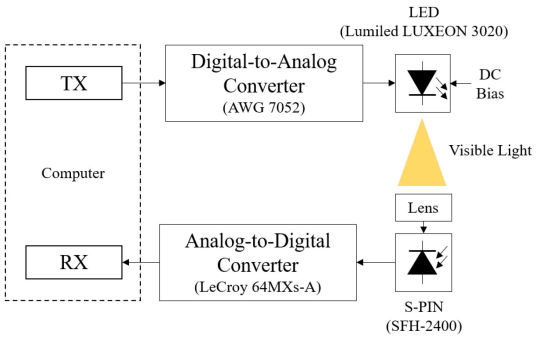

(a)

(b)

Fig. 12. Experimental VLC setup: (a) diagram and (b) picture.

TABLE I
SYSTEM PARAMETERS

Parameter	Value
LED 3-dB modulation bandwidth	1.47 MHz
Semi-angle at half luminance $\theta_{\frac{1}{2}}$	55°
DC bias current	120 mA
LED output luminous flux	53 lm
Photodiode responsivity at 870 nm	0.65 A/W
Photodiode active surface	1 mm^2
Lens diamater	16 mm
Link distance	20 cm
Illumination level	500 lx
Upsampling factor K	4
SRRC filter length	40 symbol periods
LED dynamic range	0 - 240 mA
Noise PSD N_0	-116 dBm/Hz

Fig. 13. Note, bit rates of 135 Mbps and 99 Mbps were chosen in this case for 64-CAP and 8-PAM respectively, so that the nonlinearity can be differentiated from the noise in the constellation and eye diagram. The impact of LED nonlinearity in 64-CAP is characterized by asymmetrical distortions on the bottom left and top right edge of the received constellation as shown in Fig. 13(a), whereas in 8-PAM, the nonlinear distortions are characterized by a narrower spacing of amplitude levels in the upper and lower parts of the eye diagram as can be seen in Fig. 13(c). Moreover, as shown in Fig. 13(b) and (d), the postdistortion algorithm effectively mitigates the nonlinearity.

Secondly, we perform an experimental transmission of 8-PAM and 64-CAP at the same bit rate, namely 210 Mbps, for various values of roll-off factor α. It should be noted that at this bit rate, the power margin is around 4.8 dB for each modulation scheme, according to simulation results. The transmitted frame comprises 80000 known symbols. At the receiver, the FSE-DFE equalizer coefficients are optimized based on the least mean squares (LMS) algorithm. Moreover, the coefficients of the postdistorter are obtained after a training phase using the RLS

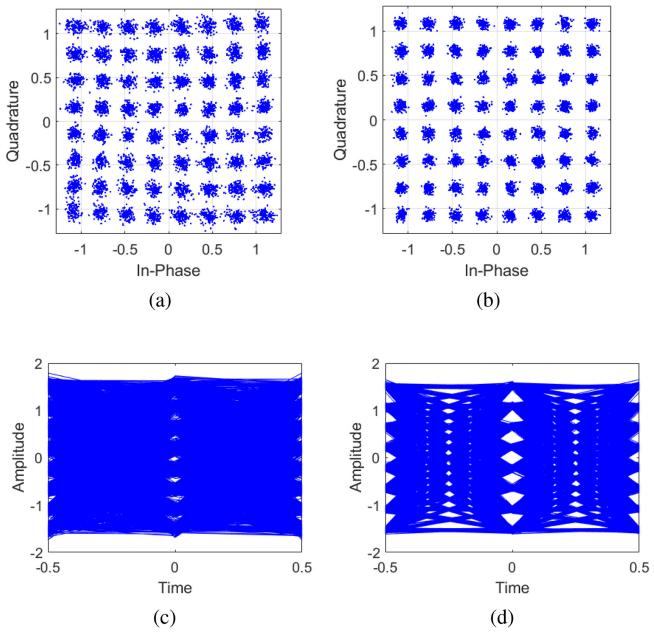

Fig. 13. Received constellation diagrams for 135 Mbps 64-CAP signal without (a) and with (b) nonlinearity mitigation, and eye diagrams for 99 Mbps 8-PAM signal without (c) and with (d) nonlinearity mitigation.

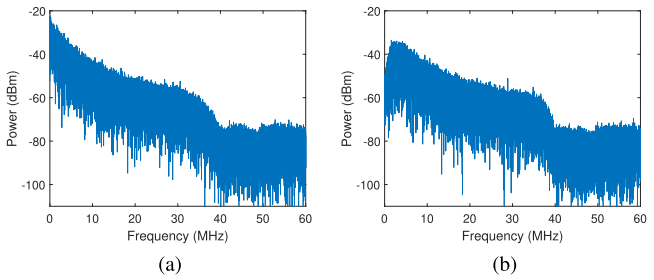

Fig. 14. Received sepctra for 210 Mbps 8-PAM (a) and 64-CAP (b) signals.

algorithm, and the memory length is set to 17 as a trade-off between performance and complexity.

The received spectra of the 210 Mbps transmission with 64-CAP and 8-PAM are shown in Fig. 14 and the BER performance is plotted in Fig. 15. First, it can be seen that without nonlinearity compensation, 8-PAM provides the poorest BER performance regardless of the value of the roll-off factor, and the calculated BER is around $\sim 2.1 \times 10^{-2}$, whereas it is $\sim 3 \times 10^{-3}$ for 64-CAP. Therefore, in practice, CAP modulation with high modulation orders provides lower BER than PAM when nonlinearity compensation is absent. On the other hand, when the LED nonlinear distortions are mitigated, the 64-CAP signal suffers more degradation compared to 8-PAM, which supports the simulation results in IV-B. For instance, for $\alpha = 0.2$, the BER performance drops from 4.2×10^{-2} to 3.4×10^{-4} for 8-PAM and from 3×10^{-3} to 8.7×10^{-4} for 64-CAP.

Furthermore, when postdistortion is applied, the BER performance of 8-PAM improves when the roll-off factor increases from 0.15 to 0.4 while that of 64-CAP becomes poorer, which is in line with the results provided by the simulation and presented in Fig. 11(c) and (f).

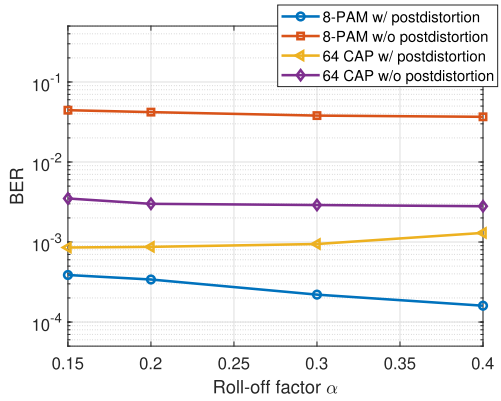

Fig. 15. BER performance of 64-CAP and 8-PAM for various roll-off factors with compensation of the nonlinearity (w/ postdistortion) and without compensation (w/o postdistortion).

These results can be contrasted with [6] where low-level PAM is recommended over CAP because of the inherent robustness of the former scheme against nonlinear distortions. However, when high modulation orders are employed in the context of high speed communication, CAP exhibits more robustness compared to PAM against nonlinear distortions. Moreover, these results highlight the necessity of postdistortion for high-order PAM and CAP.

C. Comparison With Previous DMT Experiments

Other than in the case of PAM and CAP, DMT is a multicarrier modulation technique where the signal bandwidth is divided into subcarriers onto which are mapped quadrature amplitude modulation (QAM) complex symbols. With knowledge of the channel state, power allocation and bit loading algorithms can be employed to benefit as much as possible from the available modulation bandwidth and therefore maximize the system throughput for a target BER [30]. DMT offers the advantage of simple equalization since a single-tap equalizer is needed to compensate the effects of the flat fading channel experienced by each subcarrier, whereas a more complex equalizer is required for PAM and CAP to cope with ISI, such as FSE-DFE.

In a previous study from 2020 [10], an experiment was carried out with DMT under identical conditions and using the same experimental setup. Without compensating LED nonlinearity, a $\sim$ 100 Mbps transmission rate was successfully achieved at a BER of 10^{-3}, which is significantly less than the achievable transmission rates demonstrated in this study with PAM and CAP. A major reason for the difference of performance is the high PAPR in DMT. In fact, bilateral amplitude clipping must be applied to fit the signal within the dynamic range of the LED, at the expense of clipping noise. In addition, the LED nonlinear distortions on the time-domain DMT signal generate inter-carrier interference, which degrades the overall system performance.

For comparison purposes against PAM and CAP, let us assess the achievable bit rate of DMT when LED nonlinearity distortion is mitigated. To this end, DMT pilots with 512 subcarriers loaded with QAM symbols are sent through the VLC system. The

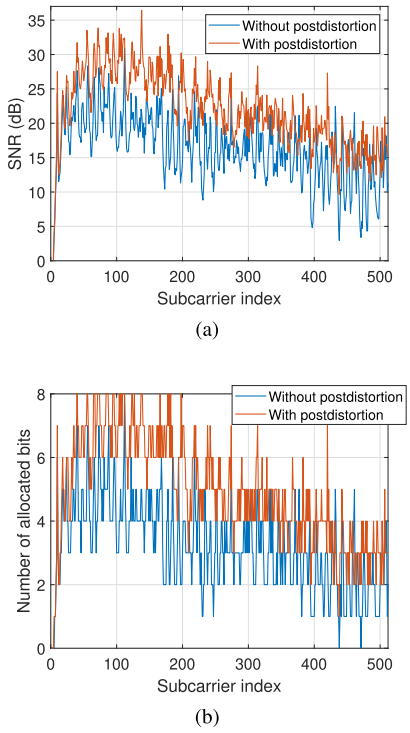

Fig. 16. SNR (a) and number of allocated bits (b) per subcarrier.

sampling frequency of the AWG generator is set to 120 MS/s. At the receiver, the SNR per subcarrier for a target BER of 10^{-3} is calculated and the number of allocated bits per subcarrier is computed using Chow's algorithm. The results are presented in Fig. 16(a) and (b). It can be observed that the SNR per subcarrier is significantly improved when the impact of LED nonlinearity is mitigated with the postdistorter, and the total number of allocated bits in one DMT symbol increases from 1646 to 2526. As a result, considering the cost of the cycling prefix set to 33 samples, the achievable practical transmission bit rate is $\sim$ 95 Mbps and $\sim$ 145 Mbps without and with nonlinearity compensation, respectively. By comparing these results with that of V-B, it can be concluded that DMT provides lower throughput than PAM and CAP.

VI. Conclusion

In this paper, two modulation schemes were compared through simulation and experiment, namely PAM and CAP employing a low-cost white LED and meeting the requirements of illumination standards for indoor lighting. It appeared that typical indoor lighting requirements lead to a sufficiently high SNR to enable transmission with high-order PAM and high-order CAP such as 8-PAM or 64-CAP. The impact of the roll-off factor on the system performance was also studied. It is shown that a small value of roll-off factor (i.e., 0.15) is preferred to achieve maximum throughput and reduce bandwidth requirements. However, when no bandwidth limitation is imposed by the electronic circuitry, the optimum value is around 0.4 for PAM and 0.15 for CAP. The simulation results indicate a slight advantage for PAM over CAP in terms of achievable throughput. The achievable data rates for both modulation formats are nonetheless similar, and are on the order of a few hundred Mbps.

It was also found that the LED nonlinearity has a significant impact on the system performance when employing PAM and CAP with a large constellation size, and that the two modulation schemes are affected differently by the nonlinear distortions. Adaptive postdistortion based on the Volterra series expansion was implemented to cope with the nonlinear behavior of the LED in practice. The performance of highly spectral-efficient modulation schemes such as 8-PAM and 64-CAP were analyzed with and without postdistortion. In conclusion, the nonlinear distortions can severely degrade the performance of 8-PAM, whereas 64-CAP shows more robustness. However, when the VLC system is linearized by the postdistorer, 8-PAM is the most suitable modulation scheme. In addition, our results indicate that high-order CAP and PAM with postdistortion perform substantially better than DMT in terms of achievable transmission rate and are suitable for high-speed VLC systems under illumination constraints. In this paper, the performance study focused on single-band CAP and PAM modulation, which offer very good performance in terms of low PAPR in relation with our initial requirements. A future and interesting extension of this work would consist in performing an optimization of multi-band CAP with adaptive bit-loading, as well as variants of DMT such as DFT-S-OFDM, which has the virtue of reducing the signal PAPR.

References

[1] N. Chi, *LED-Based Visible Light Communications, ser. Signals and Communication Technology*, Berlin, Germany: Springer, 2018.
[2] Z. Ghassemlooy, L. N. Alves, S. Zvanovec, and M.-A. Khalighi, *Visible Light Communications, Theory and Applications*. Boca Raton, FL, USA: CRC Press, 2017.
[3] D. Karunatilaka, F. Zafar, V. Kalavally, and R. Parthiban, "LED based indoor visible light communications: State of the art," *IEEE Commun. Surveys Tuts.*, vol. 17, no. 3, pp. 1649–1678, Jul.–Sep. 2015.
[4] International Energy Agency, "Lighting sales by type in the sustainable development scenario 2010-2030," 2020. [Online]. Available: https://www.iea.org/data-and-statistics/charts/lighting-sales-by-type-in-the-sustainable-development-scenario-2010-2030
[5] J.-Y. Sung, C.-W. Chow, and C.-H. Yeh, "Is blue optical filter necessary in high speed phosphor-based white light LED visible light communications?," *Opt. Exp.*, vol. 22, no. 17, pp. 20646–20651, Aug. 2014, Art. no. 20646.
[6] G. Stepniak, L. Maksymiuk, and J. Siuzdak, "Experimental comparison of PAM, CAP, and DMT modulations in phosphorescent white LED transmission link," *IEEE Photon. J.*, vol. 7, no. 3, Jun. 2015, Art. no. 7901708.
[7] M.-A. Khalighi, S. Long, S. Bourennane, and Z. Ghassemlooy, "PAM- and CAP-based transmission schemes for visible-light communications," *IEEE Access*, vol. 5, pp. 27002–27013, 2017.
[8] G. Stepniak, M. Schuppert, and C.-A. Bunge, "Advanced modulation formats in phosphorous LED VLC links and the impact of blue filtering," *J. Lightw. Technol.*, vol. 33, no. 21, pp. 4413–4423, Nov. 2015.
[9] S. Dimitrov and H. Haas, *Principles of LED Light Communications*. Cambridge, U.K.: Cambridge Univ. Press, 2015.
[10] A. Jabban, S. Haese, and M. Helard, "Theoretical and experimental optimization of DMT-based visible light communication under lighting constraints," *EURASIP J. Wireless Commun. Netw.*, vol. 2020, no. 1, pp. 1–29, Dec. 2020.
[11] R. D. Gitlin and S. B. Weinstein, "Fractionally-spaced equalization: An improved digital transversal equalizer," *Bell Syst. Tech. J.*, vol. 60, no. 2, pp. 275–296, 1981.

[12] G.-H. Im, D. Harman, G. Huang, A. Mandzik, M.-H. Nguyen, and J.-J. Werner, "51.84 Mb/s 16-CAP ATM LAN standard," *IEEE J. Sel. Areas Commun.*, vol. 13, no. 4, pp. 620–632, May 1995.

[13] K. O. Akande, P. A. Haigh, and W. O. Popoola, "On the implementation of carrierless amplitude and phase modulation in visible light communication," *IEEE Access*, vol. 6, pp. 60532–60546, 2018.

[14] N. Anous, T. Ramadan, M. Abdallah, K. Qaraqe, and D. Khalil, "Impact of blue filtering on effective modulation bandwidth and wide-angle operation in white LED-based VLC systems," *OSA Continuum*, vol. 1, no. 3, pp. 910–929, Nov. 2018.

[15] H. Le Minh *et al.*, "100-Mb/s NRZ visible light communications using a postequalized white LED," *IEEE Photon. Technol. Lett.*, vol. 21, no. 15, pp. 1063–1065, Aug. 2009.

[16] T. Luan and K. Qian, "Research on influencing factors of LED frequency response," in *Proc. AIP Conf.*, 2017, vol. 1864, no. 1, Art. no. 020008.

[17] K. Ying, Z. Yu, R. J. Baxley, H. Qian, G.-K. Chang, and G. T. Zhou, "Nonlinear distortion mitigation in visible light communications," *IEEE Wireless Commun.*, vol. 22, no. 2, pp. 36–45, Apr. 2015.

[18] S. Long, "Indoor channel modeling and high data rate transmission for visible light communication systems," Ph.D. dissertation, Fresnel Inst., École Centrale de Marseille, France, Sep. 2016.

[19] G. Stepniak, J. Siuzdak, and P. Zwierko, "Compensation of a VLC phosphorescent white LED nonlinearity by means of Volterra DFE," *IEEE Photon. Technol. Lett.*, vol. 25, no. 16, pp. 1597–1600, Aug. 2013.

[20] Y. Wang, L. Tao, X. Huang, J. Shi, and N. Chi, "Enhanced performance of a high-speed WDM CAP64 VLC system employing Volterra series-based nonlinear equalizer," *IEEE Photon. J.*, vol. 7, no. 3, pp. 1–7, Jun. 2015.

[21] H. Qian, S. J. Yao, S. Z. Cai, and T. Zhou, "Adaptive postdistortion for nonlinear LEDs in visible light communications," *IEEE Photon. J.*, vol. 6, no. 4, pp. 1–8, Aug. 2014, Art. no. 7901508.

[22] J.-K. Lain and Y.-H. Chen, "An ANN-based adaptive predistorter for LED nonlinearity in indoor visible light communications," *Electronics*, vol. 10, no. 8, 2021, Art. no. 948.

[23] X. Li, Q. Gao, C. Gong, and Z. Xu, "Nonlinearity mitigation for VLC with an artificial neural network based equalizer," in *Proc. IEEE Glob. commun. Workshops*, 2018, pp. 1–6.

[24] P. Miao, B. Zhu, C. Qi, Y. Jin, and C. Lin, "A model-driven deep learning method for LED nonlinearity mitigation in OFDM-based optical communications," *IEEE Access*, vol. 7, pp. 71436–71446, 2019.

[25] Y. Zhou *et al.*, "Comparison of nonlinear equalizers for high-speed visible light communication utilizing silicon substrate phosphorescent white LED," *Opt. Exp.*, vol. 28, no. 2, pp. 2302–2316, 2020.

[26] W. Zhao, "Nonlinearity modelling and mitigation for LED communications," Ph.D. dissertation, School Elect., Comput. Telecommun. Eng., Univ. Wollongong, Australia, 2018.

[27] G. Stepniak, M. Kowalczyk, and J. Siuzdak, "Volterra kernel estimation of white light LEDs in the time domain," *Sensors*, vol. 18, no. 4, 2018, Art. no. 1024.

[28] Z. Ghassemlooy, W. Popoola, and S. Rajbhandari, *Optical Wireless Communications: System and Channel Modelling With MATLAB*, 2nd ed. Boca Raton, FL, USA: CRC Press, 2018.

[29] *Light and Lighting - Lighting of Work Places. Part 1: Indoor Work Places*, European Committee for Standardization, Standard EN 12464-1, 2011.

[30] L. Peng, M. Hélard, and S. Haese, "On bit-loading for discrete multi-tone transmission over short range POF systems," *J. Lightw. Technol.*, vol. 31, no. 24, pp. 4155–4165, Dec. 2013.